Inorganic Chemistry

ARTICLE

pubs.acs.org/IC

Balance between Fluorescence Enhancement and Association Affinity in Fluorescent Heteroditopic Indicators for Imaging Zinc Ion in Living Cells

Gui-Chao Kuang,[†] John R. Allen,[‡] Michelle A. Baird,[‡] Brian T. Nguyen,[†] Lu Zhang,[†] Thomas J. Morgan, Jr.,[§] Cathy W. Levenson,[§] Michael W. Davidson,*[,‡] and Lei Zhu*[,†]

[†]Department of Chemistry and Biochemistry, Florida State University, Tallahassee, Florida 32306-4390, United States

[‡]National High Magnetic Field Laboratory and Department of Biological Science, Florida State University, 1800 East Paul Dirac Drive, Tallahassee, Florida 32310, United States

[§]College of Medicine, Florida State University, 1115 West Call Street, Tallahassee, Florida 32306-4300, United States

Supporting Information

ABSTRACT: A fluorescent heteroditopic indicator for the zinc(II) ion possesses two different zinc(II) binding sites. The sequential coordination of zinc(II) at the two sites can be transmitted into distinct fluorescence changes. In the heteroditopic ligand system that our group developed, the formations of mono- and dizinc(II) complexes along an increasing gradient of zinc(II) concentration lead to fluorescence enhancement and an emission bathochromic shift, respectively. The extents of these two changes determine the sensitivity and, ultimately, the effectiveness of the heteroditopic indicator in quantifying zinc(II) ion over a large concentration range. In this work, a strategy to increase the degree of fluorescence enhancement upon the formation of the monozinc-(II) complex of a heteroditopic ligand under simulated physiological conditions is demonstrated. Fluorination of the pyridyl groups in the pentadentate *N*,*N*,*N*′-tris(pyridylmethyl)ethyleneamino group reduces the apparent pK_a value of the high-affinity site, which increases the degree of fluorescence enhancement as the monozinc(II) complex is forming. However, fluorination impairs the coordination strength of the high-affinity zinc(II) binding site, which in the triply fluorinated ligand reduces the binding strength to the level of the low-affinity 2,2′-bipyridyl. The potential of the reported ligands in imaging zinc(II) ion in living cells was evaluated. The subcellular localization properties of two ligands in five organelles were characterized. Both benefits and deficiencies of these ligands were revealed, which provides directions for the near future in this line of research.

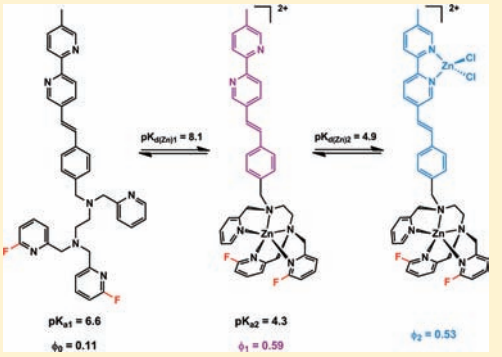

INTRODUCTION

A fluorescent heteroditopic ligand contains two metal coordination sites; one has a higher affinity, or a different selectivity, than the other. Over the concentration gradient of a metal ion (M in Figure 1), one or two of the three coordination states—non-, mono-, and dicoordinated—predominates, which upon excitation expresses distinct steady-state fluorescence as a function of metal ion concentration within a broad range (Figure 1).[1,2] A fluorescent heteroditopic ligand by design undergoes a number of relaxation processes upon photoexcitation, including electron transfer, energy transfer, or fluorescence.[1,3] The relative rates of these processes are acutely dependent on the coordination status of the ligand.[4] The construction of a fluorescent heteroditopic ligand that is capable of generating a large fluorescence contrast between its three coordination states is fundamentally interesting and challenging, because such an exercise requires a precise, and oftentimes improved understanding of the relevant stepwise coordination chemistry and its effect on the photophysical properties of the ligand, as well as the impact of the environment (e.g., solvent, counterion, etc.) on the coordination chemistry and photophysical profiles of the ligand.

As early as 2000, modulation of the fluorescence of a heteroditopic ligand via sequential metal coordination was observed by Rurack et al.[2,5−7] It was suggested that such a platform could be applied in sensing technologies that have large concentration coverage or multiplexed capabilities. The potential ability of a fluorescent heteroditopic ligand to cover a large sensing or imaging concentration range is particularly relevant to the studies of biological zinc(II) ion,[8−18] whose concentration may vary from a subnanomolar regime to approaching millimolar on certain occasions.[19] In the resting states of most mammalian cells, the free or mobile zinc(II)[20] concentrations in cytosol are at nanomolar or lower levels.[20−22] In certain zinc(II)-storing subcellular

Received: August 8, 2011
Published: September 12, 2011

vesicular structures (e.g., those found in hippocampal mossy fiber neuron terminals), the concentrations of free zinc(II) are much higher.[23,24] When cells are subjected to environmental changes, free zinc(II) concentrations may increase drastically due to the stimulated release of zinc(II) from zinc(II)-storing vesicles. For example, when insulin is released from pancreatic β cells, the corelease of zinc(II) leads to a rapid increase of extracellular concentration of free zinc(II).[25] When hippocampal neurons are under stimulation, the flow of neural transmitter glutamate to the synaptic cleft prior to entering the postsynaptic neuron is accompanied by zinc(II) ion.[26−28] These events involve large swings of concentrations of zinc(II), for which indicators with single zinc(II) binding sites are unable to cover.[29]

The use of two indicators that are effective in two different concentration regimes may collectively record the full profiles of zinc(II) dynamics during these events. This approach has been demonstrated on several occasions.[30−32] However, the use of two or multiple indicators may suffer uneven cellular uptake efficiencies and/or varied subcellular localization properties. Therefore, a single indicator with broad concentration coverage is advantageous in quantitative profiling of zinc(II) distribution and dynamics when large swings of zinc(II) concentration occur. The fluorescent heteroditopic ligand platform promises to produce indicators with large zinc(II) concentration coverage for quantitative biological sensing/imaging purposes.

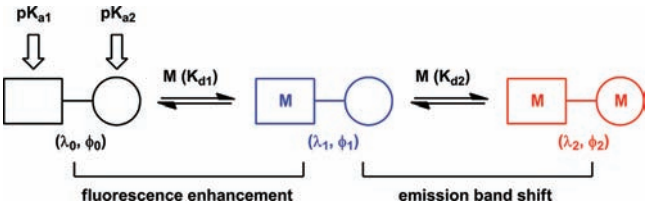

Figure 1. Metal coordination-dependent fluorescence of a fluorescent heteroditopic ligand. Square, high-affinity binding site; circle, low-affinity binding site; M, the metal ion of interest, in this study zinc(II); λ, emission wavelength; ϕ, fluorescence quantum yield. Subscripts denote the coordination status. In this work, the monozinc(II) complex formation results in a fluorescence enhancement, whereas the dizinc(II) complex formation leads to an emission band shift. K_a and K_d are the acidity constant and the metal complex dissociation constant, respectively, of a metal coordination site. "1" and "2" denote the high- and low-affinity site, respectively.

Our group reported fluorescent heteroditopic ligand **1** (Figure 2), whose fluorescence is dependent on free zinc(II) concentration over a range of 6 orders of magnitude under zinc(II)-buffered, pH-neutral aqueous conditions.[33] Compound **1** contains a phenylvinyl−bipyridyl fluorophore whose fluorescence is quenched via intramolecular photoinduced electron transfer (PET)[34] from the amino groups in the high-affinity pentadentate metal coordination site (boxed in blue). Zinc(II) coordination at the high-affinity site lowers the rate of PET, hence allowing the fluorescence to occur. The formation of the dizinc(II) complex at high zinc(II) concentrations leads to a bathochromic shift of emission due to the stabilization of a charge-transferred excited state by the presence of the zinc(II) ion.[35]

The fluorescence enhancement factor, defined as the ratio of the fluorescence quantum yields of the monozinc(II) complex and the free ligand (ϕ_1/ϕ_0), and the emission band shift ($\Delta\lambda$) are the two metrics used in evaluating the heteroditopic indicator in a sensing/imaging context.[4] A large $\Delta\lambda$ may allow the use of two separate fluorescence microscopic filter sets to record the intensity changes in both fluorescence channels. A large ϕ_1/ϕ_0 is imperative for creating an indicator that is highly sensitive to the variation of free zinc(II) within low concentration regimes (i.e., nanomolar or below). For compound **1** under physiological conditions, the values of ϕ_1/ϕ_0 and $\Delta\lambda$ are 1.9 and 30 nm, respectively. Developing strategies to increase $\Delta\lambda$ of a heteroditopic indicator is the topic of a separate project.[3] Herein, we introduce a solution to increase the fluorescence enhancement factor ϕ_1/ϕ_0 of **1**. We will also evaluate the live-cell imaging potentials of the family of fluorescent heteroditopic indicators derived from the structure of compound **1**.

RESULTS AND DISCUSSION

A. Design. The fluorescence quantum yield of compound **1** under zinc(II)-free physiological conditions is 0.30.[33] We

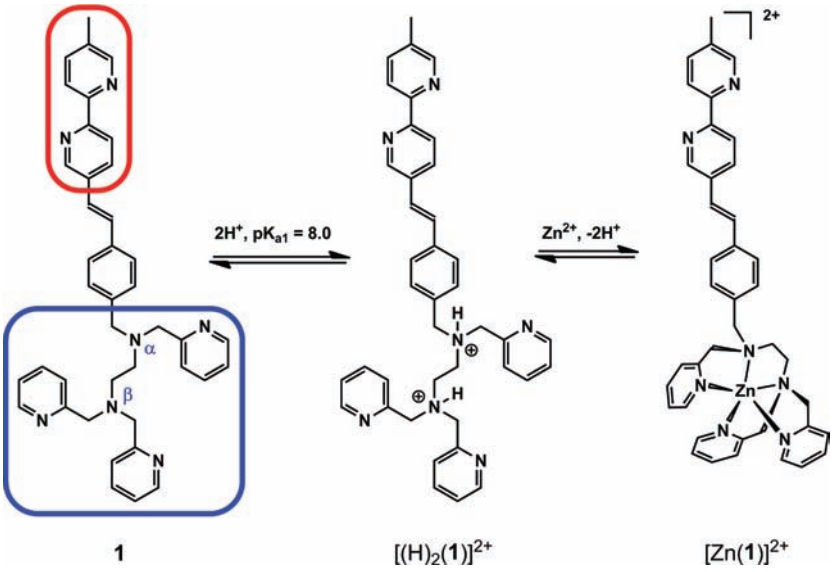

Figure 2. The protonation of the high-affinity binding site of ligand **1** and the formation of the monozinc(II) complex. Blue and red frames box the high- and low-affinity binding sites, respectively.

dx.doi.org/10.1021/ic201728f |*Inorg. Chem.* 2011, 50, 10493–10504

Chart 1. Structures

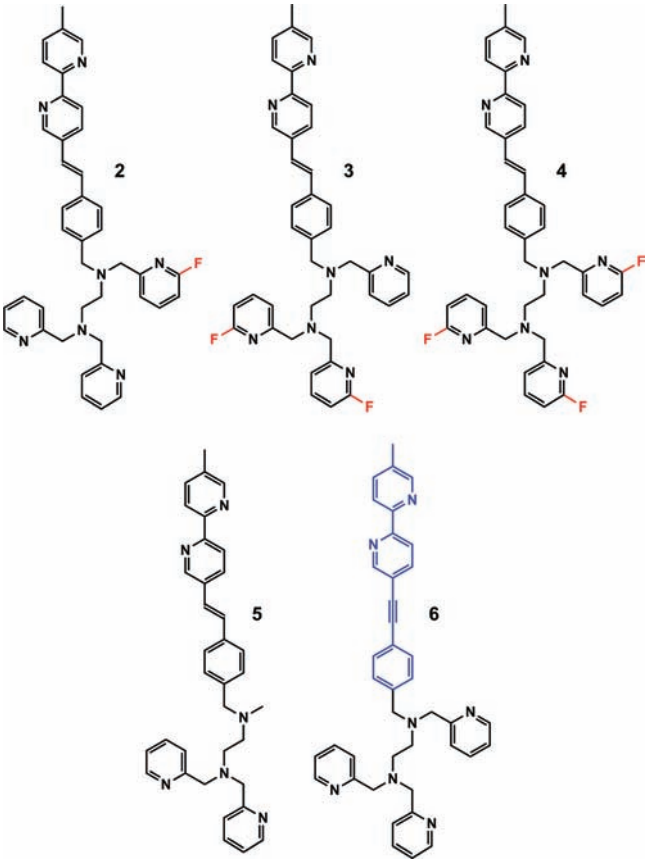

hypothesized that the protonation of the electron-donating tertiary amino groups reduces the efficiency of PET, which results in high background fluorescence (Figure 2). Therefore, decreasing the pK_a of the amino groups by strategically installing electron-withdrawing components in proximity shall increase the efficiency of PET, hence lowering the background fluorescence.

Two strategies were devised for raising the electron-withdrawing capability of the substituents on the amino groups: (1) The double-bond in **1** is replaced with a triple bond to afford compound **6**. Not only the electron-withdrawing ability of the fluorophore, which is covalently attached to the amino quencher via a methylene group, is enhanced, but the possibly interfering alkene photoisomerization process is eliminated.[36] (2) The electron-withdrawing fluorine is placed on the pyridyl groups within the high-affinity binding site to result in compounds **2**−**4** (see Chart 1). This design shall selectively lower the pK_a of the amino groups without altering the photophysical properties of the phenylvinyl−bipy fluorophore in **1**.[37]

B. Synthesis. The syntheses of fluorinated ligands **2**−**4** are shown in Scheme 1. 2-Fluoro-6-bromomethylpyridine (**7**)[38] undergoes an S_N2 substitution with *N*,*N*-dipicolyl-1,2-ethylenediamine (**8**)[39] to afford the monofluorinated pentadentate ligand **9**. Reductive amination between compounds **9** and **15** results in ligand **2**. The difluorinated *N*,*N*-di(2-fluoro-6-pyridylmethyl)-ethylenediamine (**12**) was prepared using the two-step sequence developed for compound **8**.[39] Compound **12** subsequently undergoes reductive amination with 2-pyridinecarboxaldehyde or a substitution reaction with compound **7** to afford pentadentate ligands **13** and **14**, respectively. Ligands **3** and **4** were obtained following the reductive amination reactions of **13** and **14** with aldehyde **15**. The preparations of nonfluorinated compounds **5** and **6** are described in the Supporting Information.

C. pH Profiles of the Ligands. Due to the structural similarity of heteroditopic ligands **1**−**6**, monofluorinated ligand **2** is chosen as an example in the following description of the investigation on the pH dependence of fluorescence. There are five different (six overall, as marked by arrows in Figure 3) protonatable sites within the pH range of 2−10 in ligand **2**, which challenges the determination of the pH-fluorescence profile. In the six protonatable sites, two are tertiary amino groups and four are pyridyl/6-fluoropyridyl groups. The acid/base equilibria of four sites are expected to impact the fluorescence property of ligand **2**: the protonation of the tertiary amino groups (marked by blue arrows) would inhibit the fluorescence quenching PET processes, whereas the protonation of the bipy (2,2′-bipyridyl) nitrogen atoms (marked by red arrows) would enhance the charge-transfer character of the fluorophore. We do not expect the protonation of the other three unconjugated pyridyl/6-fluoropyridyl groups (marked by green arrows) to significantly affect the fluorescence of **2**. Since the pK_a values of a tertiary amino and a pyridyl group are well-separated, we should be able to use two apparent pK_a values for the tertiary amino containing high-affinity binding site (pK_{a1} in Figure 1) and the bipy-containing low-affinity binding site (pK_{a2} in Figure 1), respectively, to characterize the pH-fluorescence profile of ligand **2**.

The fluorescence of ligand **2** rises as pH decreases from 9.9. After the intensity maximizes at a pH ∼ 5.3, the emission undergoes a bathochromic shift as the solution turns further acidic (Figure 4A). Similar to the fluorescence response of the heteroditopic ligand to a zinc(II) gradient,[1] the high-affinity site is protonated during the first phase (starting from pH 9.9 downward), which results in a fluorescence enhancement, whereas the protonation of the low-affinity bipy site in the second phase leads to the bathochromic shift of the emission. The two-phase transition that the fluorescence of ligand **2** experiences as pH decreases from 9.9 to 2.0 can be monitored at two different wavelength channels (Figure 4B). By fitting the portions of largest changes of the three isotherms[40] with a modified Henderson−Hasselbalch equation (see details in the Supporting Information), the apparent pK_a values of the high- (note that in the high-affinity site there are two amino groups which are difficult to distinguish) and low-affinity binding sites of ligand **2** were determined (Table 1). The pK_a values of other ligands (Table 1) were obtained using the same approach.

As shown in Table 1, the substitution of fluorine on the pyridyl groups in the high-affinity binding site of **1** to afford ligands **2**−**4** reduces the pK_a value of the high-affinity site (pK_{a1}) without significantly altering that of the low-affinity site (pK_{a2}). Single fluorine substitution (compound **2**) on the pyridyl group attached to the amino group two bonds away from the fluorophore (N(α) in Figure 2) reduces the pK_{a1} value by 1.7 unit (from 8.0 to 6.3). Double-fluorination (compound **3**) on the two pyridyl groups attached to the amino group further away from the fluorophore (N(β) in Figure 2) has a similar effect on pK_{a1}. Triple-fluorination further reduces the pK_{a1} to 6.0 in compound **4**, thus resulting in a pentadentate ligand that is largely unprotonated at neutral pH. The pK_{a2} value drops slightly upon fluorine substitution at the high-affinity site, up to 0.2 unit in the triply fluorinated ligand **4**. The replacement of N(α)-picolyl in **1** with a N(α)-methyl group, which results in compound **5**,

dx.doi.org/10.1021/ic201728f |*Inorg. Chem.* 2011, 50, 10493–10504

Scheme 1. Reagents and Conditions: (a) dry ethanol, K_2CO_3, reflux, 1 h, 25%; (b) 15, $NaBH(OAc)_3$, rt, 6 h; (c) dry ethanol, Na_2CO_3, reflux, 5 h, 74%; (d) TFA, CH_2Cl_2, rt, 1.5 h, 95%; (e) 2-pyridinecarboxaldehyde, $NaBH(OAc)_3$, rt, 6 h, 36%; (f) 7, dry ethanol, K_2CO_3, reflux, 3 h, 22%

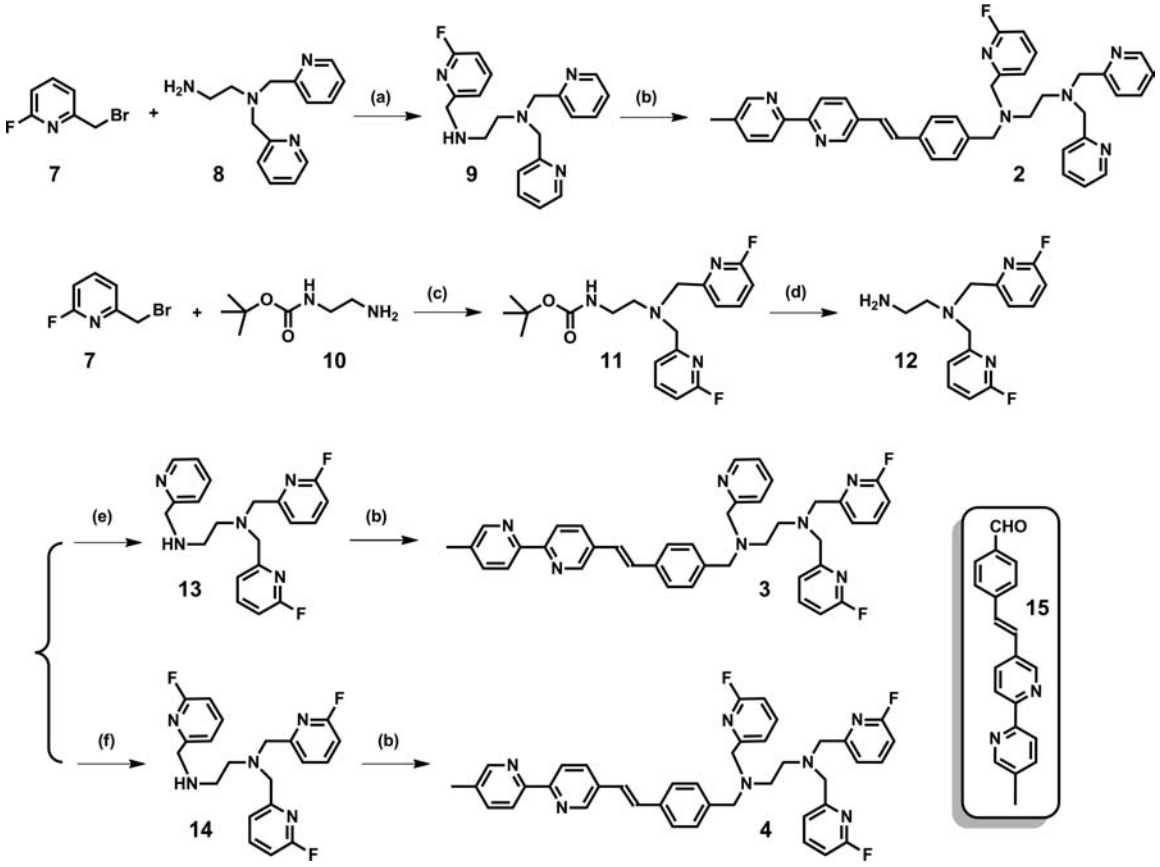

raises the pK_{a1} value to 8.8, suggesting that the 2-picolyl group is more electron-withdrawing than the methyl group.

The pK_a effect on the background fluorescence (in the absence of zinc(II) addition) of a ligand at a physiological pH of 7.4 can be assessed using the ratio of integrated fluorescence intensity at a pH of 7.4 and the maximum intensity achievable over a pH gradient (e.g., at pH 5.3 for ligand **2**, see Figure 4A). The values of $I_{7.4}/I_{max}$ of ligands **1**−**6** are listed in Table 1. Fluorination at the high-affinity site suppresses the background fluorescence ($I_{7.4}/I_{max} \leq 33\%$ of **2**−**4**), while $I_{7.4}/I_{max}$ of nonfluorinated ligand **1** is 69%. In the case of the nonfluorinated ligand **5**, the $I_{7.4}/I_{max}$ is 96%, indicating that there is little room for further enhancement upon binding zinc(II). It was later shown from the zinc(II) titration experiment that the addition of zinc(II) only reduces the fluorescence of the solution containing ligand **5**.

The formal oxidation of the carbon−carbon double bond in **1** to a triple bond in **6** also decreases the basicity of the amino group N(α), which has a pK_{a1} value of 7.3. This strategy on raising the electron-withdrawing ability of the fluorophore is similar to that developed by Lippard et al. where fluorination of the xanthene fluorophore moiety lowers the pK_a of the di(2-picolyl)amino-based zinc(II) binding site in the zinpyr series of indicators.[41] Structural modification of the fluorophore in **1** to afford **6** also decreases the basicity of the bipy low-affinity site so that the pK_{a2} value drops to 4.0. The formal oxidation of the fluorophore reduces the charge-transfer character of the fluorophore,[36] which

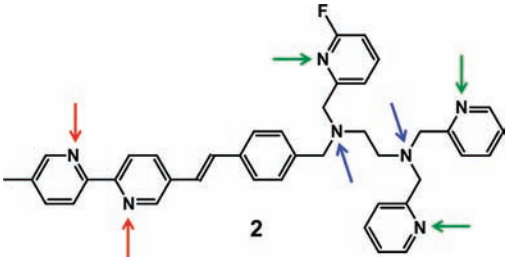

Figure 3. The protonatable sites in ligand **2** (marked by arrows). The blue arrows represent the tertiary amino groups. The red arrows represent the bipy nitrogens. The green arrows represent the unconjugated pyridyl groups.

creates shorter excitation (320 nm) and emission (380 nm) wavelengths and a smaller emission band shift (~20 nm) upon zinc(II) coordination (see section E). The excitation and emission profiles fall into the UV region, which challenges the glass-based conventional fluorescence microscopes that we apply in cell imaging experiments. Therefore, compound **6** was not considered an indicator for zinc(II) in imaging applications.

D. Comments on the Metal Buffering System. Before we present the zinc(II)-coordination data of compounds **1**−**6** in the next section, some comments on the solvent system that we used in the study are warranted. The dissociation constants of the ligand/zinc(II) complexes were determined under metal-buffered

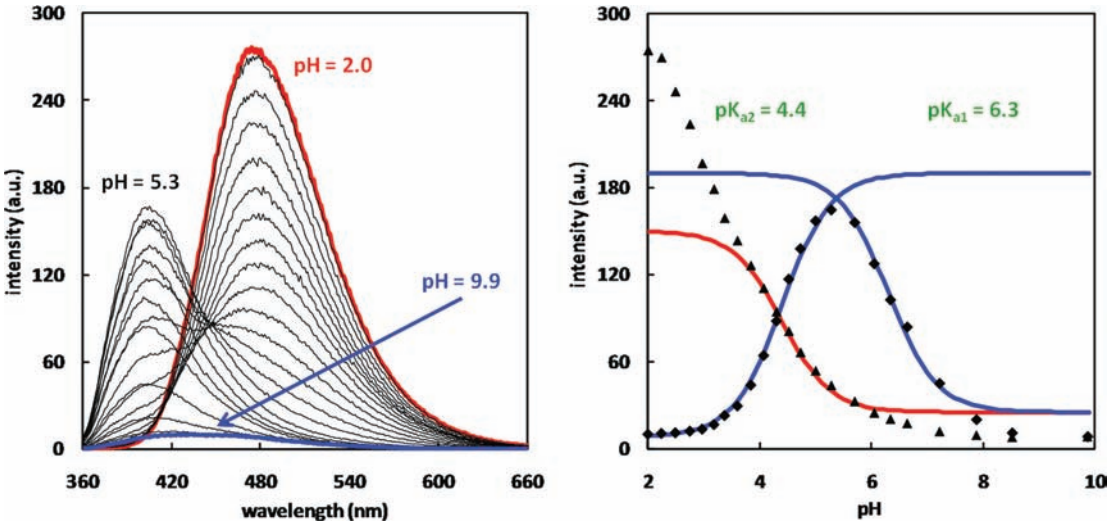

Figure 4. (A) Fluorescence spectra of **2** (5.5 μM, λ_{ex} = 350 nm) collected at various pH's (conditions: 10% DMSO, [mixed pH buffer] = 90 mM (see Supporting Information), [EGTA] = 9 mM). Blue and red spectra were acquired at the highest pH and the lowest pH values, respectively. (B) The fluorescence intensity dependence on pH at 400 nm (diamonds) and 470 nm (triangles). Blue and red lines are fitting curves based on a modified Henderson−Hasselbalch equation. The fitted apparent pK_a values are listed in green.

neutral aqueous conditions, where the total zinc(II) concentration ($[Zn]_t$) remains high (close to millimolar level). However, since the majority of zinc(II) ions are bound by the metal cheletor (or metal buffer) in the solution, the free zinc(II) (unbound from organic ligands, hydrated zinc(II) ion)[20] is kept at much lower levels. Therefore, this situation mimics that in the intracellular milieu, where total zinc(II) abundance is high, while the majority of it is associated with zinc(II)-binding proteins.[20,42] The fluctuation in the free zinc(II) concentration ($[Zn]_f$) may stimulate the release or uptake of zinc(II) by zinc(II)-binding proteins, such as metallothionein,[20,43,44] to offset the change, therefore creating a buffering system that is pivotal in maintaining zinc(II) homeostasis required for proper physiological functions.

The interplay between the zinc(II) ion, the metal buffer, and the indicator can be understood by analyzing the following two equilibria. K_d' and K_d represent the dissociation constants of zinc(II) with the metal buffer and the indicator, respectively.

$$Zn^*buffer \leftrightarrow Zn^{2+} + buffer$$
$$K_d' = \frac{[Zn]_f[buffer]}{[Zn^*buffer]} \quad (1)$$

$$Zn^*ind \leftrightarrow Zn^{2+} + ind$$
$$K_d = \frac{[Zn]_f[ind]}{[Zn^*ind]} \quad (2)$$

Assuming that the total indicator concentration ($[ind]_t$) is 2 μM,

$$[ind]_t = [ind] + [Zn^*ind] = 2\ \mu M$$

When [ind] = [Zn*ind] = 1 μM, where $[Zn]_f$ falls at the center of the effective coverage of the indicator, $[Zn]_f = K_d$, which, in this demonstration, is within the nanomolar range or below. Under such conditions, the total Zn^{2+} concentration

$$[Zn]_t = [Zn]_f\ (nM) + [Zn^*ind]\ (\mu M) + [Zn^*buffer]\ (mM)$$

Table 1. pK_a Values of High- and Low-Affinity Binding Sites of 1−6[a]

pK_a	1	2	3	4	5	6
high-affinity (pK_{a1})	8.0	6.3	6.6	6.0	8.8	7.3
low-affinity (pK_{a2})	4.4	4.4	4.3	4.2	4.6	4.0
$I_{7.4}/I_{max}$[b]	69%	27%	33%	15%	96%	60%

[a] The curve-fitting plots based on fluorescence titration data of ligands **1**, **3**−**6** are included in the Supporting Information. [b] The ratio of integrated fluorescence intensity at pH 7.4 over the maximal intensity achievable in the blue channel.

where $[Zn]_f$ is in the nanomolar range, [Zn*ind] is in the micromolar range, and [Zn*buffer] is in the millimolar range. Therefore, $[Zn]_t \approx$ [Zn*buffer], yet $[Zn]_f$ is controlled in the nanomolar range via equilibrium (eq 1). What the indicator is reporting is $[Zn]_f$ under zinc(II)-buffered conditions in the presence of a large zinc(II) reservoir, where the presence of a minuscule amount of the indicator does not affect the $[Zn]_f$ that is controlled according to eq 1. Under the described thermodynamically equilibrating zinc(II)-buffered conditions, assuming a 1:1 binding stoichiometry between the indicator and zinc(II), the fluorescence intensity measured at various $[Zn]_f$'s is independent of the indicator concentration as shown by Tsien et al. in analogous studies of calcium(II)-buffered systems (eq 3), when I_{min} and I_{max} are known.[45] The zinc(II)-buffering system has been applied to characterize a large number of zinc(II) indicators[20,31,42,46−71] that operate under physiological conditions. However, we feel that a clear clarification and a justification to a broader audience for applying the metal-buffered conditions in characterizing zinc(II) indicators for biological uses are needed on the basis of the questions that we have received over the past few years regarding the appropriateness of this particular experimental approach. We consider that the application of zinc(II)-buffered conditions generates more reproducible affinity data than a direct titration between zinc(II) and an indicator, because the zinc(II)-buffered system significantly reduces the effect of interfering metal ions and inaccuracy in indicator

dx.doi.org/10.1021/ic201728f |Inorg. Chem. 2011, 50, 10493–10504

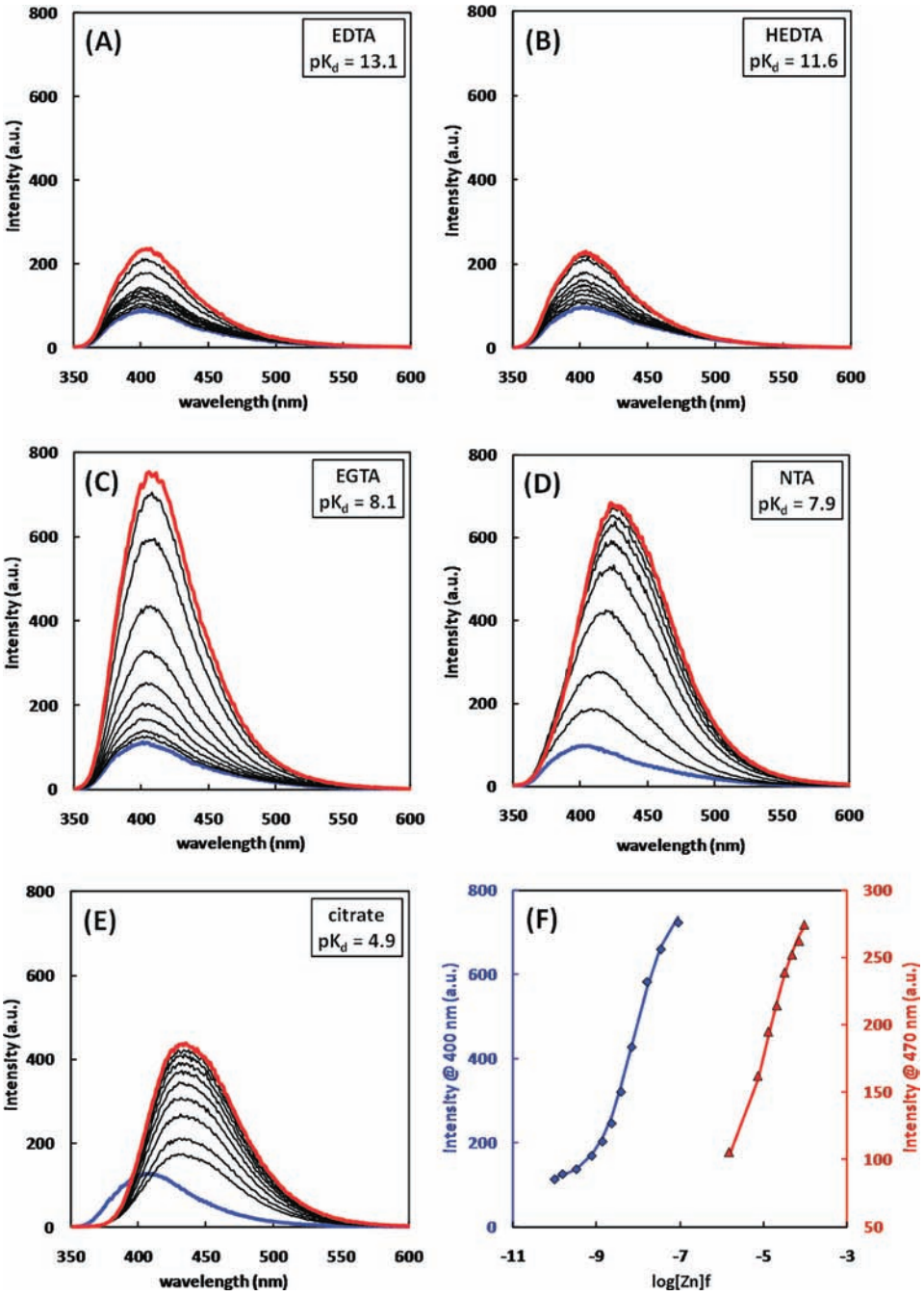

Figure 5. (A−E) Fluorescence spectra of ligand **3** (4.1 μM) in the presence of increasing $[Zn]_f$ (from blue to red traces) in the buffering ranges of EDTA, HEDTA, EGTA, NTA, and citrate, respectively. The instrumental parameters were unchanged in the titration experiments. The ranges of *y* axes are intentionally kept identical so that the data collected in the five buffered conditions can be compared. (F) Best fits of fluorescence changes using eq 3 at 400 nm (blue) and 470 nm (red) in solutions buffered by EGTA and citrate, respectively.

concentration measurement in affinity determinations, in addition to providing an environment that is close to physiological conditions for studying the coordination chemistry of zinc(II).

$$I = \frac{(I_{min}K_d + I_{max}[Zn])}{(K_d + [Zn])} \quad (3)$$

When the conditions to establish the zinc(II)-buffered environment do not hold, the correlation between fluorescence intensity and $[Zn]_f$ could not be described by the Tsien equation (eq 3). The breakdown of the zinc(II)-buffered conditions would take place when (1) the solution is not sufficiently buffered for metal ions (e.g., when the indicator concentration is high enough to affect the buffering system),[72] (2) the chemical or biochemical event under investigation is not in a thermodynamic equilibrium (e.g., when zinc(II) concentration spikes up and down on a time scale that is faster than the association or dissociation rate of the zinc(II)−indicator complex), or (3) a 1:1 binding stoichiometry cannot be used to approximate the association between the indicator and zinc(II).

E. Zinc(II) Titration Experiments in Metal-Buffered Aqueous Solutions. The zinc(II) titration experiments were carried out in aqueous solutions (pH 7.4) where the $[Zn]_f$ was buffered in different ranges applying the following five metal chelators: EDTA ($K_d = 7.6 \times 10^{-14}$ M), HEDTA ($K_d = 2.3 \times 10^{-12}$ M), EGTA ($K_d = 7.8 \times 10^{-9}$ M), NTA ($K_d = 1.4 \times 10^{-8}$ M), and citrate ($K_d = 1.2 \times 10^{-5}$ M).[73] Five fluorescence titration experiments were carried out for each of the ligands **1**−**6** in aqueous solutions that contained individual metal chelators within their respective buffering ranges. The data were used to *estimate* the zinc(II) affinities, assuming a 1:1 coordination stoichiometry, of the high- and low-affinity sites of **1**−**6**.

The analysis of the zinc(II) binding profile of difluorinated indicator **3** (Figure 5) is described as an example. The increases of $[Zn]_f$ within the buffering ranges of EDTA (Figure 5A) and HEDTA (Figure 5B) lead to only modest fluorescence enhancement, suggesting that the high-affinity site of ligand **3** has a smaller affinity constant than those of EDTA and HEDTA ($K_{d1} > K_{d(EDTA\ or\ HEDTA)}$). The fluorescence of **3** responds to $[Zn]_f$ variation sensitively in the solution buffered by EGTA, indicating that K_{d1} is on par with that of the EGTA/zinc(II) complex. When NTA is used to control $[Zn]_f$, fluorescence enhancement and bathochromic shift occur simultaneously, implying that both high- and low-affinity sites of **3** can be populated in this particular range of $[Zn]_f$. In the citrate-buffered solution, the fluorescence spectrum immediately shifts to a longer wavelength with the addition of zinc(II), indicating the rapid saturation of the high-affinity binding site and the coordination at the bipy secondary site. On the basis of the data in Figure 5, the apparent 1:1 binding constant between zinc(II) and the high-affinity binding site of ligand **3** (K_{d1}) was satisfactorily fitted using the titration trace at 400 nm collected in EGTA-buffered solution (blue in Figure 5F). The zinc(II) affinity assuming a 1:1 binding stoichiometry of the bipy low-affinity site (K_{d2}) was estimated[74] by fitting the titration trace at 470 nm collected in the citrate-buffered solution.

Other ligands (**1**, **2**, **4**−**6**) were analyzed using the same approach. The curve fittings of ligand **1** in both EDTA- and HEDTA-buffered solutions were satisfactory (Figure S6, Supporting Information). Therefore, the pK_{d1} ($-\log K_{d1}$) of ligand **1** was calculated as the average of the values determined in the two titration experiments. The pK_{d1} of ligand **2** was best fitted in a titration experiment using a solution containing both HEDTA and EGTA (Figure S7, Supporting Information). The fluorescence of ligand **4** does not change much in buffers containing chelators EDTA, HEDTA, EGTA, and NTA (Figure S8, Supporting Information), suggesting that triple-fluorination significantly decreases the affinity of the high-affinity site to zinc(II). Therefore, only one dissociation constant was reported for ligand **4**, which was determined in the citrate-buffered solution. Unlike ligands **1**−**4**, no fluorescence enhancement was observed in the titration experiments involving ligand **5** (Figure S9, Supporting Information), where a methyl group replaces the 2-picolyl group at N(α) close to the fluorophore. As shown in Table 1, the high-affinity site of ligand **5** is almost fully protonated at pH 7.4, which restores the fluorescence of **1** that is quenched via the PET pathway in the unprotonated form. Therefore, little fluorescence alteration occurs when the high-affinity site of **5** takes up zinc(II). The fluorescence quantum yields and emission maxima of non-, mono-, and dicoordinated forms of ligands **1**−**6** as well as their dissociation constants are listed in Table 2.

Fluorination of the high-affinity binding site of ligand **1** lowers its affinity to zinc(II) (see the values of pK_{d1} of ligands **1** and **6** vs those of ligands **2**−**4** in Table 2). In the triply fluorinated ligand **4**, the affinity of the high-affinity, pentadentate site drops to the level that is indistinguishable from the bidentate bipy low-affinity site. On the other hand, fluorination on the high-affinity site of **1** does drop the apparent pK_{a1} value, thus increasing the fluorescence enhancement factor (ϕ_1/ϕ_0 in Table 2) from 1.9 of the nonfluorinated ligand **1** to 5.4 of the difluorinated ligand **3**. The fluorination at the high-affinity site does not appear to affect the photophysical properties of the fluorophore as the emission maxima of the free and zinc(II)-bound forms are similar in ligands **1**−**5**. In ligand **6**, the triple-bond-containing fluorophore possesses a lesser degree of internal charge transfer (ICT) character than the phenylvinyl−bipy fluorophore in the other ligands.[36] Therefore, the zinc(II)-coordination-enabled emission bathochromic shift of **6** is smaller than those of **1**−**5**.

Table 2. Fluorescence Quantum Yields (ϕ_0−ϕ_2) and Emission Band Maxima (λ_1, λ_2) of 1−6, and the Dissociation Constants (pK_{d1}, pK_{d2}) of Their Mono- and Di-Zinc(II) Complexes under Metal-Buffered Aqueous Conditions

ligand	pK_{d1}	pK_{d2}	ϕ_0[a]	ϕ_1[a]	ϕ_2[a]	ϕ_1/ϕ_0	λ_1/nm[b]	λ_2/nm[b]	$\Delta\lambda$/nm[c]
1	12.8	5.2	0.30	0.57	0.65	1.9	405	433	28
2	9.5	5.2	0.23	0.64	0.75	2.8	405	433	28
3	8.1	4.9	0.11	0.59	0.53	5.4	402	434	32
4	ND[d]	5.4	0.14	ND[d]	0.52	ND[d]	400	430	30
5	ND[d]	6.2	0.44	0.43	0.64	0.98	398	427	29
6	12.8	~5.2	0.17	0.48	0.35	2.8	380	401	21

[a] ϕ_0, ϕ_1, and ϕ_2 are fluorescence quantum yields of free ligand, monozinc(II) complex, and dizinc(II) complex, respectively. [b] λ_1 and λ_2 are the short and long emission band maxima, respectively. [c] $\Delta\lambda = \lambda_2 - \lambda_1$. [d] ND: not determined.

F. Potentials of Ligands 1 and 3 in Imaging Zinc(II) in Living Cells. Compounds **1**−**5** show little toxicity as determined using an In Vitro Toxicology Assay Kit (sulforhodamine B based; Sigma Tox-6). HeLa (S3) cells were incubated in either DMEM (Dulbecco's Modified Eagle Medium) or HBSS (Hank's Buffered Salt Solution) in the presence of various ligand molecules up to 10 μM, which is beyond the upper limit of the concentration range of the indicator used in the fluorescence imaging experiments. There is no apparent cell toxicity in DMEM during the first 6 h of incubation as measured by SRB (Figures S11−20, Supporting Information). After 24 h, various degrees of cell decline that are proportional to the dosage of the indicators were observed. The ligands show little toxicity in HBSS, in which the HeLa (S3) cells were treated with the ligands for up to 6 h. We concluded that the toxicity of ligands **1**−**5** at low micromolar loading concentrations is insignificant over the time scale of the imaging experiments, which last up to 1 h.

The abilities of ligands **1**−**5** to fluorometrically follow mammalian intracellular zinc(II) concentration as affected by the medium zinc(II) content were evaluated using HeLa (S3) cells as a model system. Invariably, the supplementation of zinc(II) in the media drives up the intracellular fluorescence. The concentration dependence of the fluorescence intensity varies in each case. The imaging data of compounds **1** (nonfluorinated) and **3** (difluorinated) are discussed in the following text. The data collected using other ligands are included in the Supporting Information (Figures S21−23).

HeLa (S3) cells were incubated in HBSS buffer containing 2 μM of compound **1** for 30 min at 37 °C. After the indicator

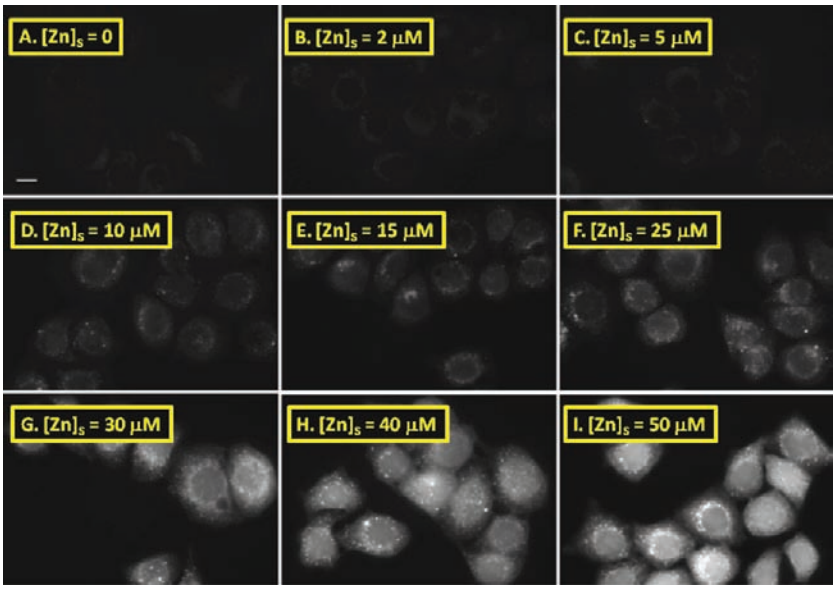

Figure 6. Fluorescent images of HeLa (S3 line) cells loaded with nonfluorinated indicator **1** (2.0 μM) in the presence of supplemental $ZnCl_2$ (0−50 μM) in HBSS. Scale bar in A = 10 μm. Excitation 355−405 nm; emission 420−480 nm.

molecules were removed by replacing fresh media (HBSS) with graded $ZnCl_2$ concentrations, the samples were imaged after 10 min of incubation at 37 °C. Imaged using the emission filter set QMax Blue, whose emission spectral window covers 420−460 nm, the collected signals primarily come from the long emission band centered at 433 nm (λ_2 in Table 2). The short-wavelength emission band of **1** centers at 405 nm, which is largely outside the detection range of the QMax Blue filter set. Upon increasing the supplemental zinc(II) concentration ($[Zn]_s$) in the media, a monotonous fluorescence enhancement was observed (Figure 6). The mean fluorescence intensity per cell was plotted against $[Zn]_s$ (Figure 7). The zinc(II)-mediated fluorescence enhancement (I/I_0) vs $[Zn]_s$ is shown in Figure S24 (Supporting Information).

During the initial phase of increasing $[Zn]_s$, the enhancement of intensity from indicator **1** is moderate. The intensity starts to increase sharply at 25 μM onward to 50 μM. We interpreted that when $[Zn]_s$ is below 20 μM, the fluorescence enhancement occurs at the shorter wavelength band which centers at 405 nm. This emission band is largely outside the coverage of the QMax Blue filter set. Therefore, little intensity change is discernible in the first three (A−C) frames. Due to the large affinity gap between the high- and low-affinity sites in **1** (pK_{d1} = 12.8, pK_{d2} = 5.2), the fluorescence intensity does not vary significantly during the intermediate range of the zinc(II) gradient (D−F). When the $[Zn]_s$ is high enough for zinc(II) to occupy the low-affinity site, the longer emission band centered at 433 nm starts to rise, which is captured by the QMax Blue filter set as seen in the last three frames (G−I) and in Figure 7.

This experiment demonstrated that the intracellular fluorescence of **1** is dependent on the concentration of supplemental zinc(II). The overall zinc(II)-mediated fluorescence enhancement is up to 17-fold, which constitutes a large signal dynamic range. The limitation of compound **1** is its inability to be analyzed by two separate emission filter sets because the emission band separation is not wide enough. Furthermore, the wavelength of the emission that responds to zinc(II) in the low concentration

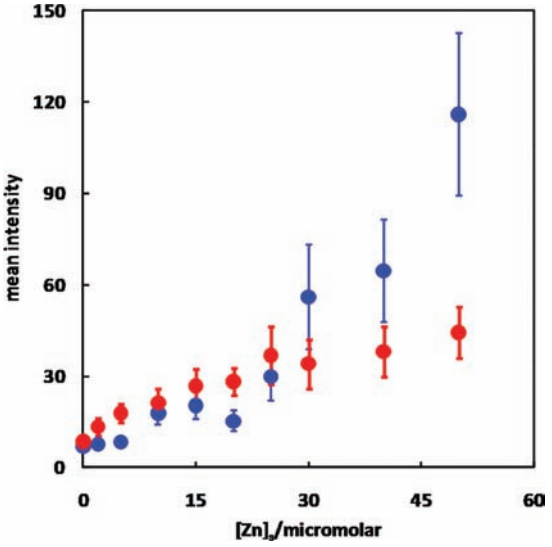

Figure 7. Mean fluorescence intensity per cell (on a scale of 0−255) of indicators **1** (blue) and **3** (red) vs supplemental $[ZnCl_2]$ ($[Zn]_s$) in the media. A minimum of 30 cells were analyzed in image J for each data point.

regime is not long enough to be captured fully using the commercial QMax Blue filter set. Therefore, the fluorescence information in the low concentration regime remains largely uncovered. These limitations will be addressed in the next phase of this project.

The difluorinated ligand **3** also displays a fluorescence enhancement over an increasing zinc(II) gradient (Figure 8). The dynamic range (Figure 7, red trace) is smaller compared to that of the nonfluorinated **1**. The intracellular distribution is also visibly different. Ligand **3** tends to form bright particulates intracellularly. As $[Zn]_s$ increases, the density of the particulates grows, which gives rise to an overall higher mean intensity. However, because the fluorescence intensity of most of the particulates is at the

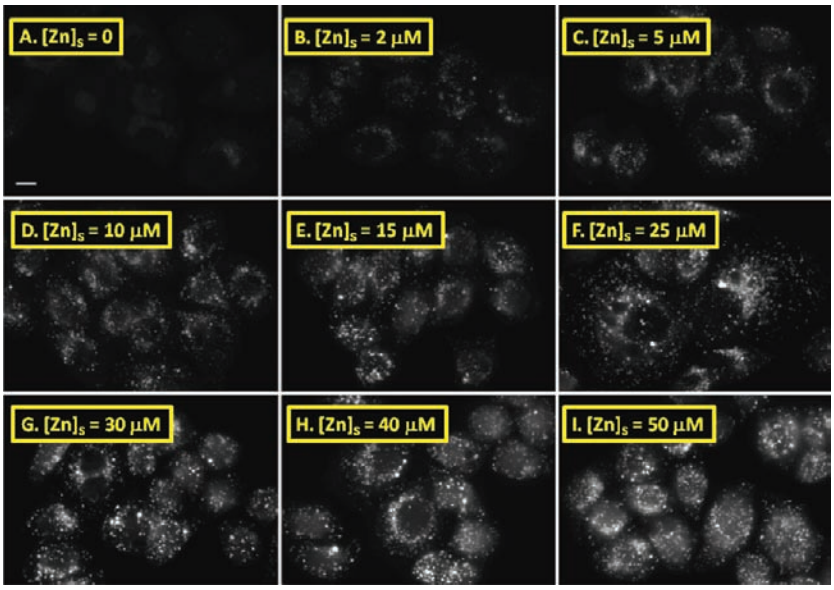

Figure 8. Fluorescent images of HeLa (S3 line) cells loaded with difluorinated indicator **3** (2.0 μM) in the presence of supplemental $ZnCl_2$ (0−50 μM) in HBSS. Scale bar in A = 10 μm. Excitation 355−405 nm; emission 420−480 nm.

Table 3. Subcellular Localization Profiles, As Represented by Pearson's Correlation Coefficients (PCC),[75] of Indicators 1 and 3 under Zinc(II)-Deficient and Zinc(II)-Enriched Conditions

	nucleus	mitochondrion	Golgi complex	endoplasmic reticulum	endosome
1	17 ± 5%	90 ± 4%	74 ± 7%	86 ± 5%	82 ± 3%
1 + Zn^{2+}	44 ± 12%	68 ± 5%	66 ± 15%	84 ± 7%	79 ± 5%
3	7 ± 7%	58 ± 10%	66 ± 10%	71 ± 8%	58 ± 5%
3 + Zn^{2+}	42 ± 7%	64 ± 5%	67 ± 8%	77 ± 4%	75 ± 7%

saturation level, the mean intensity is underestimated, which leads to an overall smaller dynamic range than that of ligand **1**. We attribute the particulate formation to the tendency of fluorinated ligands (**2**−**4**) to aggregate. This hypothesis is consistent with the observation of a long wavelength tail of the absorption spectrum of the difluorinated ligand **3** at 10 μM in a neutral aqueous solution (Figure S25A, Supporting Information), which is an indication of inadequate solubility under the applied conditions. On the basis of the concentration dependence of absorption at 480 nm (Figure S25B, Supporting Information), presumably solely arising from aggregation, we estimated that the solubilities of **1** and **3** under the working conditions are 10 μM and 2 μM, respectively. The actual origin of the fluorescence of the particulates (or aggregates) requires detailed photophysical characterization which is beyond the scope of this report.

In summary, the following beneficial features of zinc(II) indicators **1**−**5** in fluorescence imaging experiments of living cells are demonstrated: (1) Very low loading concentrations (e.g., 2 μM) are required, which provides little disturbance to the native state of the cellular sample under analysis.[72] Most reported indicators for zinc(II) including the commercial products are often recommended for use at 5 μM or higher loading levels. (2) The uptake of the indicator molecules is rapid; a 30-min incubation is sufficient. (3) The toxicities of **1**−**5** are low. On the other hand, the following deficiencies of **1**−**5** might hamper a fluorescence imaging experiment: (a) Short wavelength, high-energy excitation is needed, which leads to photobleaching over time. (b) The particulate formation of fluorinated ligands and the lack thereof of nonfluorinated **1** in living cells are difficult to predict and to characterize chemically. (c) The uncertainty in subcellular localization needs to be addressed.

High spatial resolution is one of the most distinctive advantages of fluorescence microscopy over other minimally invasive imaging methods for analyzing living biological samples.[76,77] The subcellular localization properties of ligands **1** and **3** in five organelles, nucleus, mitochondrion, Golgi complex, endoplasmic reticulum, and endosome, were characterized (Table 3). In each case, fusions of the red fluorescent protein, mCherry (610 nm emission maximum),[78] were used to determine the degree of colocalization with the indicators.

Ligand **1** shows high degrees of localization (Pearson's correlation coefficient (PCC) over 70%) in four organelles—mitochondrion (Figure 10), endoplasmic reticulum (Figures S27 and S28, Supporting Information), Golgi complex (Figures S29 and S30, Supporting Information), and endosome (Figures S31 and S32, Supporting Information). Little localization was found in the nucleus (Figure 9A−D, PCC = 17%). Upon zinc(II) supplementation at 50 μM in the media, the degree of colocalization in nuclei increases sharply (PCC = 44%; Figure 9E−H), which correlates with the slight reduction of the PCC values in the other four organelles. This correlation might indicate a translocation of the zinc(II) complex of **1** from cytoplasmic organelles to the nucleus, due to the enhanced intercalating ability of **1** upon binding zinc(II). For compound **3** (Figures S33−S42, Supporting Information), the degrees of localization are lower than those of **1** across the board. However, the PCC

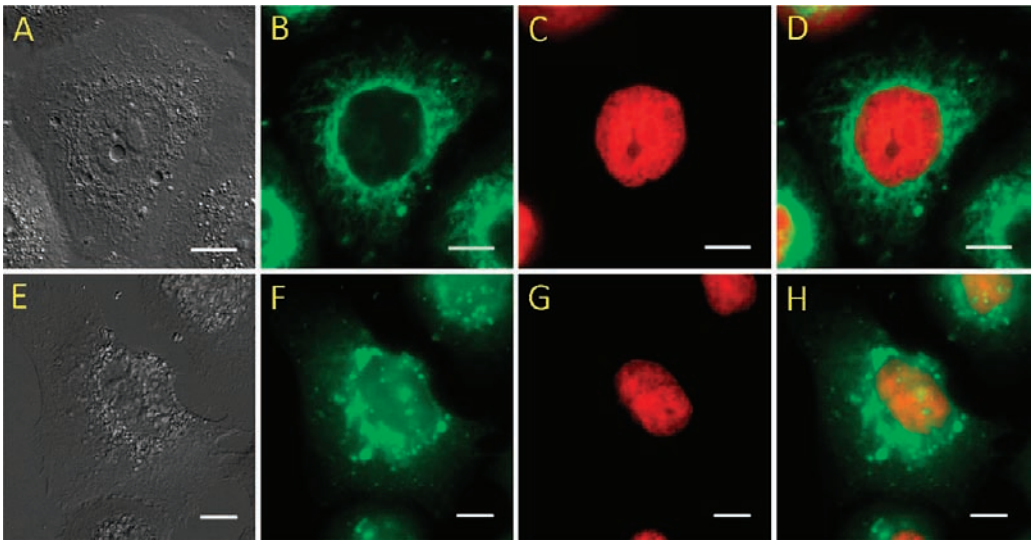

Figure 9. Images of HeLa (S3 line) cells. From left to right: DIC images; green channels representing the emission from indicator **1** (2.0 μM) captured by QMax Blue filter set (excitation 355−405 nm; emission 420−480 nm); red channels showing the emission from mCherry−H2B−N-6 that localizes in nuclei, captured by QMax Red filter set (excitation 530−570 nm, emission 600−650 nm); images after merging green and red channels. Scale bar = 10 μm. (A−D): $[Zn]_s$ = 0. (E−H): $[Zn]_s$ = 50 μM.

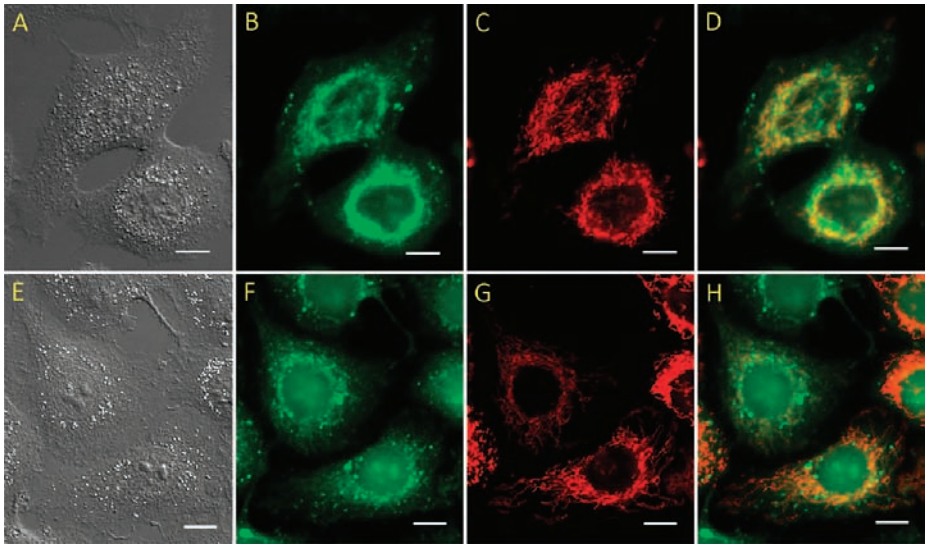

Figure 10. Images of HeLa (S3 line) cells. From left to right: DIC images; green channels representing the emission from indicator **1** (2.0 μM) captured by QMax Blue filter set (excitation 355−405 nm; emission 420−480 nm); red channels showing the emission from mCherry−PDHA1−N-10 that localize in mitochondria, captured by QMax Red filter set (excitation 530−570 nm, emission 600−650 nm); images after merging green and red channels. Scale bar = 10 μm. (A−D): $[Zn]_s$ = 0. (E−H): $[Zn]_s$ = 50 μM.

increases uniformly upon zinc(II) addition, an indication of the organelles picking up the zinc(II) complex of **3** from cytosol. The aggregates of ligand **3** in cytosol may be broken up to some degrees upon dizinc(II) complex formation, which is then distributed to various organelles, giving rise to the increase of localizations in these organelles.

SUMMARY

Heteroditopic indicators **1**−**6** are evaluated by two parameters: the fluorescence enhancement factor, which is the fluorescence quantum yield increase upon monozinc(II) complex formation, and emission band shift upon dizinc(II) complex formation. The fluorescence enhancement factor of **1** is low (ϕ_1/ϕ_0 = 1.9). In this work, we demonstrated a strategy to increase ϕ_1/ϕ_0, which consequently leads to a high sensitivity of zinc(II) quantification at a low concentration regime. We found that fluorination of the pyridyl groups in the pentadentate *N*,*N*,*N*′-tris(pyridylmethyl)ethyleneamino group in **1**, a well-known ligand for zinc(II) and an electron donor in designs of photoinduced electron transfer (PET)-switching based metal ion indicators, leads to reduced pK_a values of the ligand. Consequently, quenching via PET of the attached fluorophore, in the current case phenylvinyl−bipyridyl, becomes more efficient under pH neutral conditions, which leads to a larger fluorescence enhancement

when zinc(II) binds. On the other hand, overfluorination, such as in the triply fluorinated ligand **4**, leads to a much reduced zinc(II) ion affinity of the pentadentate ligand. The fluorinated pentadentate ligands introduced in this work could be readily grafted to other metal ion receptor scaffolds. The pK_a of the ligand and the metal ion affinity (K_d) have to be balanced in choosing the strategy of fluorinating the pyridyl group on the basis of the possible concentration range of zinc(II) in a particular zinc(II) sensing application.

The potential of ligands **1**−**5** in imaging zinc(II) in living cells was assessed. All ligands permeate through the cell membrane readily. Little toxicity was observed over the time frame of the imaging experiments. The ligands show the ability to report intracellular zinc(II) variations via fluorescence change. The loading level is as low as 2 μM, lower than the recommended dosage of most currently known indicators for zinc(II). The major deficiencies of these indicators are also revealed. The tendency of fluorinated ligands to aggregate complicates the interpretation of the fluorescence observation. More importantly, the uncertainty in subcellular localization of the reported indicators, as well as most products reported in literature, compromises the unique capacity of modern fluorescence microscopy for high resolution imaging. The need for developing organelle-specific indicator molecules to complement the growing spatial resolution achievable by the state-of-art fluorescence microscopy has been noted in recent reviews.[17,79] Several groups have recently reported various strategies in developing organelle-specific indicators for zinc(II),[80−84] which will undoubtedly elevate the utilities of synthetic indicators in studying intracellular zinc(II) distribution and dynamics at organellar levels. Addressing these deficiencies is the focus of the ongoing work in our laboratory.[85]

■ ASSOCIATED CONTENT

Supporting Information. Procedures for syntheses, characterizations of new compounds, and additional spectra and images. This material is available free of charge via the Internet at http://pubs.acs.org.

■ AUTHOR INFORMATION

Corresponding Author

*E-mail: davidson@magnet.fsu.edu, lzhu@chem.fsu.edu.

■ ACKNOWLEDGMENT

This work was supported, in part, by a New Investigator Research grant from the James and Esther King Biomedical Research Program administered by the Florida Department of Health (08KN-16), National Science Foundation (CHE0809201), and National Institute of General Medical Sciences (R01GM08-1382). We thank J. Tyler Simmons for determining the aqueous solubility of ligands **1** and **3**.

■ REFERENCES

(1) Zhang, L.; Clark, R. J.; Zhu, L. *Chem.—Eur. J.* **2008**, *14*, 2894–2903.
(2) Zhu, L.; Zhang, L.; Younes, A. H. *Supramol. Chem.* **2009**, *21*, 268–283.
(3) Wandell, R. J.; Younes, A. H.; Zhu, L. *New J. Chem.* **2010**, *34*, 2176–2182.
(4) Younes, A. H.; Zhang, L.; Clark, R. J.; Davidson, M. W.; Zhu, L. *Org. Biomol. Chem.* **2010**, *8*, 5431–5441.
(5) Rurack, K.; Bricks, J. L.; Schulz, B.; Maus, M.; Reck, G.; Resch-Genger, U. *J. Phys. Chem. A* **2000**, *104*, 6171–6188.
(6) Rurack, K.; Koval'chuck, A.; Bricks, J. L.; Slominskii, J. L. *J. Am. Chem. Soc.* **2001**, *123*, 6205–6206.
(7) For more published examples, see ref 2.
(8) For review articles in the past decade on the topic of zinc(II) sensing and imaging, see refs 8−18. Kimura, E.; Aoki, S. *Biometals* **2001**, *14*, 191–204.
(9) Kikuchi, K.; Komatsu, H.; Nagano, T. *Curr. Opin. Chem. Biol.* **2004**, *8*, 182–191.
(10) Jiang, P.; Guo, Z. *Coord. Chem. Rev.* **2004**, *248*, 205–229.
(11) Lim, N. C.; Freake, H. C.; Bruckner, C. *Chem.—Eur. J.* **2005**, *11*, 38–49.
(12) Thompson, R. B. *Curr. Opin. Chem. Biol.* **2005**, *9*, 526–532.
(13) Chang, C. J.; Lippard, S. J. *Met. Ions Life Sci.* **2006**, *1*, 321–370.
(14) Dai, Z.; Canary, J. W. *New J. Chem.* **2007**, *31*, 1708–1718.
(15) Carol, P.; Sreejith, S.; Ajayaghosh, A. *Chem. Asian J.* **2007**, *2*, 338–348.
(16) Nolan, E. M.; Lippard, S. J. *Acc. Chem. Res.* **2009**, *42*, 193–203.
(17) Tomat, E.; Lippard, S. J. *Curr. Opin. Chem. Biol.* **2010**, *14*, 225–230.
(18) Xu, Z.; Yoon, J.; Spring, D. R. *Chem. Soc. Rev.* **2010**, *39*, 1996–2006.
(19) Frederickson, C. J. *Int. Rev. Neurobiol.* **1989**, *31*, 145–238.
(20) See an interpretation of "free" or "mobile" zinc(II): Krężel, A.; Maret, W. *J. Biol. Inorg. Chem.* **2006**, *11*, 1049–1062.
(21) Outten, C. E.; O'Halloran, T. V. *Science* **2001**, *292*, 2488–2492.
(22) Finney, L. A.; O'Halloran, T. V. *Science* **2003**, *300*, 931–936.
(23) Frederickson, C. J.; Klitenick, M. A.; Manton, W. I.; Kirkpatrick, J. B. *Brain Res.* **1983**, *273*, 335–339.
(24) Assaf, S. Y.; Chung, S.-H. *Nature* **1984**, *308*, 734–736.
(25) Qian, W.-J.; Aspinwall, C. A.; Battiste, M. A.; Kennedy, R. T. *Anal. Chem.* **2000**, *72*, 711–717.
(26) Li, Y.; Hough, C. J.; Suh, S. W.; Sarvey, J. M.; Frederickson, C. J. *J. Neurophysiol.* **2001**, *86*, 2597–2604.
(27) Sindreu, C. B.; Varoqui, H.; Erickson, J. D.; Pérez-Clausell, J. *Cereb. Cortex* **2003**, *13*, 823–829.
(28) Frederickson, C. J.; Koh, J.-Y.; Bush, A. I. *Nat. Rev. Neurosci.* **2005**, *6*, 449–462.
(29) Que, E. L.; Domaille, D. W.; Chang, C. J. *Chem. Rev.* **2008**, *108*, 1517–1549.
(30) Shults, M. D.; Pearce, D. A.; Imperiali, B. *J. Am. Chem. Soc.* **2003**, *125*, 10591–10597.
(31) Komatsu, K.; Kikuchi, K.; Kojima, H.; Urano, Y.; Nagano, T. *J. Am. Chem. Soc.* **2005**, *127*, 10197–10204.
(32) Nolan, E. M.; Jaworski, J.; Okamoto, K.-I.; Hayashi, Y.; Sheng, M.; Lippard, S. J. *J. Am. Chem. Soc.* **2005**, *127*, 16812–16823.
(33) Zhang, L.; Murphy, C. S.; Kuang, G.-C.; Hazelwood, K. L.; Constantino, M. H.; Davidson, M. W.; Zhu, L. *Chem. Commun* **2009**, 7408–7410.
(34) de Silva, A. P.; Moody, T. S.; Wright, G. D. *Analyst* **2009**, *134*, 2385–2393.
(35) Younes, A. H.; Zhang, L.; Clark, R. J.; Zhu, L. *J. Org. Chem.* **2009**, *74*, 8761–8772.
(36) Zhang, L.; Zhu, L. *J. Org. Chem.* **2008**, *73*, 8321–8330.
(37) See an example of fluorine substitution in altering the coordination chemistry of a pyridyl-containing multidentate ligand: Sumalekshmy, S.; Henary, M. M.; Siegel, N.; Lawson, P. V.; Wu, Y.; Schmidt, K.; Bredas, J.-L.; Perry, J. W.; Fahrni, C. J. *J. Am. Chem. Soc.* **2007**, *129*, 11888–11889.
(38) Kuang, G.-C.; Michaels, H. A.; Simmons, J. T.; Clark, R. J.; Zhu, L. *J. Org. Chem.* **2010**, *75*, 6540–6548.
(39) Kawabata, E.; Kikuchi, K.; Urano, Y.; Kojima, H.; Odani, A.; Nagano, T. *J. Am. Chem. Soc.* **2005**, *127*, 818–819.
(40) The fluorescence at the high and low ends of the pH range deviates from the fitting. At the low end, the two pyridyl moieties in bipy

are individually protonated, thus breaking the planarity of the fluorophore to affect the fluorescence. At the high end of the pH range, the aggregation of the ligand may have become an issue which affects its fluorescence. Therefore, the fitting of the data in the range of 7.5−3.5, which is the pH range of interest in this study and related fluorescence microscopy experiments, affords the best estimates of the pK_a values of the two metal coordination sites.

(41) Chang, C. J.; Nolan, E. M.; Jaworski, J.; Burdette, S. C.; Sheng, M.; Lippard, S. J. *Chem. Biol.* **2004**, *11*, 203–210.

(42) Bozym, R. A.; Thompson, R. B.; Stoddard, A. K.; Fierke, C. A. *ACS Chem. Biol.* **2006**, *1*, 103–111.

(43) Krężel, A.; Maret, W. *J. Am. Chem. Soc.* **2007**, *129*, 10911–10921.

(44) Krężel, A.; Maret, W. *J. Biol. Inorg. Chem.* **2008**, *13*, 401–409.

(45) Grynkiewicz, G.; Poenie, M.; Tsien, R. Y. *J. Biol. Chem.* **1985**, *260*, 3440–3450.

(46) Thompson, R. B.; Maliwal, B. P.; Fierke, C. A. *Anal. Chem.* **1998**, *70*, 1749–1754.

(47) Thompson, R. B.; Maliwal, B. P.; Fierke, C. A. *Anal. Biochem.* **1999**, *267*, 185–195.

(48) Fahrni, C. J.; O'Halloran, T. V. *J. Am. Chem. Soc.* **1999**, *121*, 11448–11458.

(49) Walkup, G. K.; Burdette, S. C.; Lippard, S. J.; Tsien, R. Y. *J. Am. Chem. Soc.* **2000**, *122*, 5644–5645.

(50) Hirano, T.; Kikuchi, K.; Urano, Y.; Higuchi, T.; Nagano, T. *J. Am. Chem. Soc.* **2000**, *122*, 12399–12400.

(51) Burdette, S. C.; Walkup, G. K.; Spingler, B.; Tsien, R. Y.; Lippard, S. J. *J. Am. Chem. Soc.* **2001**, *123*, 7831–7841.

(52) Gee, K. R.; Zhou, Z.-L.; Qian, W.-J.; Kennedy, R. T. *J. Am. Chem. Soc.* **2002**, *124*, 776–778.

(53) Gee, K. R.; Zhou, Z.-L.; Ton-That, D.; Sensi, S.; Weiss, J. H. *Cell Calcium* **2002**, *31*, 245–251.

(54) Dai, Z.; Xu, X.; Canary, J. W. *Chem. Commun.* **2002**, 1414–1415.

(55) Hirano, T.; Kikuchi, K.; Urano, Y.; Nagano, T. *J. Am. Chem. Soc.* **2002**, *124*, 6555–6562.

(56) Maruyama, S.; Kikuchi, K.; Hirano, T.; Urano, Y.; Nagano, T. *J. Am. Chem. Soc.* **2002**, *124*, 10650–10651.

(57) Burdette, S. C.; Frederickson, C. J.; Bu, W.; Lippard, S. J. *J. Am. Chem. Soc.* **2003**, *125*, 1778–1787.

(58) Chang, C. J.; Jaworski, J.; Nolan, E. M.; Sheng, M.; Lippard, S. J. *Proc. Natl. Acad. Sci. U. S. A.* **2004**, *101*, 1129–1134.

(59) Henary, M. M.; Wu, Y.; Fahrni, C. J. *Chem.—Eur. J.* **2004**, *10*, 3015–3025.

(60) Hanaoka, K.; Kikuchi, K.; Kojima, H.; Urano, Y.; Nagano, T. *J. Am. Chem. Soc.* **2004**, *126*, 12470–12476.

(61) Taki, M.; Wolfold, J. L.; O'Halloran, T. V. *J. Am. Chem. Soc.* **2004**, *126*, 712–713.

(62) Royzen, M.; Durandin, A.; Young, V. G. J.; Geacintov, N. E.; Canary, J. W. *J. Am. Chem. Soc.* **2006**, *128*, 3854–3855.

(63) Goldsmith, C. R.; Lippard, S. J. *Inorg. Chem.* **2006**, *45*, 555–561.

(64) Parkesh, R.; Lee, T. C.; Gunnlaugsson, T. *Org. Biomol. Chem.* **2007**, *5*, 310–317.

(65) Komatsu, K.; Urano, Y.; Kojima, H.; Nagano, T. *J. Am. Chem. Soc.* **2007**, *129*, 13447–13454.

(66) Wang, H.-H.; Gan, Q.; Wang, X.-J.; Xue, L.; Liu, S.-H.; Jiang, H. *Org. Lett.* **2007**, *9*, 4995–4998.

(67) Xue, L.; Wang, H.-H.; Wang, X.-J.; Jiang, H. *Inorg. Chem.* **2008**, *47*, 4310–4318.

(68) Kim, H. M.; Seo, M. S.; An, M. J.; Hong, J. H.; Tian, Y. S.; Choi, J. H.; Kwon, O.; Lee, K. J.; Cho, B. R. *Angew. Chem., Int. Ed.* **2008**, *47*, 5167–5170.

(69) Mizukami, S.; Okada, S.; Kimura, S.; Kikuchi, K. *Inorg. Chem.* **2009**, *48*, 7630–7638.

(70) Taki, M.; Watanabe, Y.; Yamamoto, Y. *Tetrahedron Lett.* **2009**, *50*, 1345–1347.

(71) Xu, Z.; Baek, K.-H.; Kim, H. N.; Cui, J.; Qian, X.; Spring, D. R.; Shin, I.; Yoon, J. *J. Am. Chem. Soc.* **2010**, *132*, 601–610.

(72) Dineley, K. E.; Malaiyandi, L. M.; Reynolds, I. J. *Mol. Pharmacol.* **2002**, *62*, 618–627.

(73) $[Zn]_f$'s were calculated using the MaxChelator program available at http://www.stanford.edu/~cpatton/webmaxc/webmaxcS.htm. Patton, C.; Thompson, S.; Epel, D. *Cell Calcium* **2004**, *35*, 427–431.

(74) Bipy may bind zinc(II) in a stoichiometry from 1:1 to 3:1 (ligand/zinc(II)) depending on the counteranion and solvent, see: Eorn, G. H.; Park, H. M.; Hyun, M. Y.; Jang, S. P.; Kim, C.; Lee, J. H.; Lee, S. J.; Kim, S.-J.; Kim, Y. *Polyhedron* **2011**, *30*, 1555–1564. In CH_3CN, a 1:1 binding stoichiometry between $ZnCl_2$ and bipy was reported. See: Younes, A. H.; Zhang, L.; Clark, R. J.; Zhu, L. *J. Org. Chem.* **2009**, *74*, 8761–8772.

(75) Dunn, K. W.; Kamocka, M. M.; McDonald, J. H. *Am. J. Physiol. Cell Physiol.* **2010**, *300*, C723–C742.

(76) Fernández-Suárez, M.; Ting, A. Y. *Nat. Rev. Mol. Cell Biol.* **2008**, *9*, 929–943.

(77) McRae, R.; Bagchi, P.; Sumalekshmy, S.; Fahrni, C. J. *Chem. Rev.* **2009**, *109*, 4780–4827.

(78) The emission of ligand **1** or **3** falls largely within 400−450 nm where mCherry barely absorbs (Figure S26, Supporting Information). Therefore, the probability of intermolecular FRET between the indicator at a micromolar concentration and mCherry is low.

(79) Domaille, D. W.; Que, E. L.; Chang, C. J. *Nat. Chem. Biol.* **2008**, *4*, 168–175.

(80) Tomat, E.; Nolan, E. M.; Jaworski, J.; Lippard, S. J. *J. Am. Chem. Soc.* **2008**, *130*, 15776–15777.

(81) Dittmer, P. J.; Miranda, J. G.; Gorski, J. A.; Palmer, A. E. *J. Biol. Chem.* **2009**, *284*, 16289–16297.

(82) Vinkenborg, J. L.; Nicolson, T. J.; Bellomo, E. A.; Koay, M. S.; Rutter, G. A.; Merkx, M. *Nat. Methods* **2009**, *6*, 737–U10.

(83) Qin, Y.; Dittmer, P. J.; Park, J. G.; Jansen, K. B.; Palmer, A. E. *Proc. Natl. Acad. Sci. U.S.A.* **2011**, *108*, 7351–7356.

(84) Masanta, G.; Lim, C. S.; Kim, H. J.; Han, J. H.; Kim, H. M.; Cho, B. R. *J. Am. Chem. Soc.* **2011**, *133*, 5698–5700.

(85) Sreenath, K.; Allen, J. R.; Davidson, M. W.; Zhu, L. *Chem. Commun.*, DOI: 10.1039/c1cc14580k.